A Comparative Study On Electronic Transport Behavior Of Silicene And B40-Nano Onions

Harleen Kaur
Guru Nanak Dev University
Jupinder Kaur (jupinderece.rsh@gndu.ac.in)
Guru Nanak Dev University
Ravinder Kumar
Guru Nanak Dev University

Research Article

Keywords: Nano-Electronics, Molecular Junctions, DFT, NEGF, Nano-Onions, Silicene, Borospherene (B40)

Posted Date: October 20th, 2021

DOI: https://doi.org/10.21203/rs.3.rs-954745/v1

Version of Record: A version of this preprint was published at Silicon on January 29th, 2022. See the published version at https://doi.org/10.1007/s12633-021-01630-2.

A Comparative Study On Electronic Transport Behavior Of Silicene And B40-Nano Onions

Harleen Kaur[1,a], Jupinder Kaur[*,a], Ravinder Kumar[2,a]

[a]Department of Electronics Technology, Guru Nanak Dev University, Amritsar, Punjab 143005, India

Address of all authors e-mail: [1]harleenrandhawa334@gmail.com, [*]jupinderece.rsh@gndu.ac.in, [2]ravinder.elec@gndu.ac.in

Abstract-

Density Functional Theory is utilized to scrutinize the electronic state of silicene and boron nano-onion which is a round compact mass formed by placing an N_{20}, C_{20}, and B_{20} fullerene within its parent atom fullerene B_{40}. NEGF was used to investigate the quantum transport at both equilibrium and non-equilibrium. Firstly, the I-V curve for both silicene and boron-based devices was studied and compared. From the results, it is concluded that boron-based devices are better than silicene. To get deeper insights into why boron-based devices are better than silicene, transport properties of boron-based devices were determined. Later on, the transport mechanism is analyzed by computing the DOS, transmission and molecular spectra, HLG, electron densities, and differential conductance when the boron nano-onion is placed between the pair of Au electrodes. The calculated results are evaluated and a comparative study is done. From the results, it is deduced that the N_{20} variant nano-onion has lesser HOMO-LUMO gap (HLG) and highest value of current in comparison to other devices. Thus, by infusing a smaller fullerene of N_{20} inside the hollow cage of B_{40} fullerene the amplification of current and conductance can be observed in Boron-nano-onion in comparison to other devices.

Keywords- Nano-Electronics, Molecular Junctions, DFT, NEGF, Nano-Onions, Silicene, Borospherene (B_{40})

1. Introduction

In the last decade, remarkable advances in the field of computing have been witnessed, especially when W. Shockley, J. Bardeen, and W. Brattain invented the first transistor at Bell Labs in December 1947 [1]. This was followed by the discovery of the first IC in the year 1958 and the invention of the first planar transistor in the same year by J. Hoerni [2-4]. In the last 40 years, bulk silicon has served as the most promising material for semiconductors. However, semiconductors have reached their physical limits. Richard P. Feynman's famous lecture in 1959, proposed "There's plenty of room at the bottom" [5]. This notion gave the idea to the electronics industry of using atoms and molecules at the microscopic level. Since then, research has been carried out widely on carbon and graphene nanotubes. Soon researchers started investigating other materials like silicene which has a similar atomic structure to graphene but comprises silicon atoms. The structure was first identified by Guzman-Verri & Lew Yan Voon in 2007 [6]. Though silicene has a similar atomic structure to graphene yet it is better than graphene and can be easily unified with current silicon-based technology and devices. Researchers have found that the electron mobility of silicene is 2.57 x 10^5 $cm^2V^{-1}s^{-1}$ [7] which is greater than the electron mobility of bulk silicon i.e 0.014 x 10^5 $cm^2V^{-1}s^{-1}$ [8]. Sasfan et.al has investigated the electronic structure and transport properties of silicene for gas sensor applications [9]. Dongqing Zou et. al investigated the transport properties of 6 zigzag chains of H or H_2 edge-hydrogenated silicene nanoribbon and OH or O edge-oxidized slices by forming a device [10]. It was deduced that edge functional groups can play a promising role in enhancing the electrical performance of SiNR- based devices. In 2018, M. Davoodianldalik et.al examined electronic, magnetic, and transport properties of silicene armchair nanoribbons and deduced that the addition of Fe monomer to silicene sheet enhances the spintronics and optoelectronic properties of Silicene [11]. Q.G Jiang et. al examined the stability of silicene nanoribbons by diffusing the barriers with H atoms [12]. It was found that the amalgamation of the H atoms with silicene nanoribbons increases the stability of the system.

Apart from the engrossing material discussed, another molecule is experimentally realized by Zhai in 2014, the B_{40} molecule. Zhai et. al synthesized boron fullerene (B_{40}) and demonstrated that it is a highly stable molecule [13]. Boron fullerenes are similar to carbon fullerenes as they can also be amalgamated from 2D boron sheets trailing the isolated pentagon rule [14]. B_{40} cage consists of two hexagonal and four heptagonal rings which can attract both acidic and basic molecules. Various researches have been conducted to elucidate its, structure, orientation, and electronic properties. Due to the exceptional properties of B_{40} fullerene, it was found to be a major development in the field of molecular electronics. In the previous research work, Zhang et. al scrutinized B_{40} fullerene with gold electrodes and deduced that it depicts optoelectronic properties [15]. The HLG of the B_{40} molecular device is reduced considerably by adding a strontium atom, which escalates the value of current through the device [16]. Because of the existence of both acidic and basic sites, B_{40} fullerene has been extensively utilized as a sensor for the detection of various toxic gases [17].

Plentiful research has been done in the field of molecular electronics based on carbon as a carbon nano-onion (CNO) yet boron fullerene (B_{40}) as boron nano-onion still needs to be explored. In this paper, we constructed a Boron Nano-Onion (BNO) by the endohedral placement of a fullerene inside parent fullerene B_{40} as shown in fig.1. Three different fullerenes (C_{20}, N_{20}, and B_{20}) were considered to be placed inside parent fullerene B_{40}. We intend to study the transport and electronic properties of boron-based nano-onion attached to gold metallic leads and also comparing it with the electron transport properties of silicene. By applying the density functional theory (DFT) as well as the non-equilibrium green's function, we aim to study the I-V curve, transmission spectra, DOS, molecular energy spectrum, eigenstates, and transmission pathways.

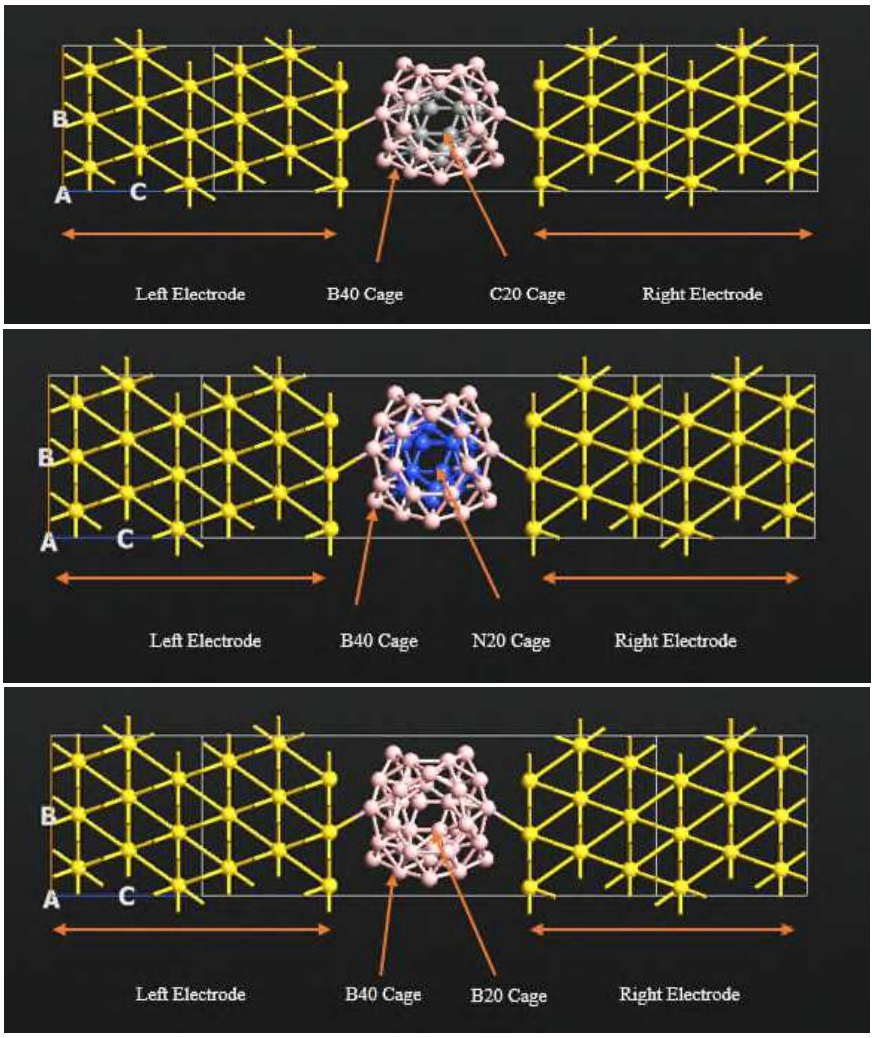

Fig.1: Pictorial representation of molecular junction (a) C_{20}@B_{40} Nano-onion (b) N_{20}@B_{40} Nano-onion (c) B_{20}@B_{40}.

2. Methodology

For a better understanding of various electronic properties, all the calculations were performed using density functional theory (DFT) [18-21]. DFT calculations were used as implemented in the Atomistix Tool kit and its graphical interface was used for simulating all the configurations [22]. Two probe devices were formed consisting of the left metallic lead (L), central scattering region (C), and right metallic lead (R). For left/right metallic leads gold was used. A molecular junction device was formed by placing a BNO molecule between the metallic leads. The electrode length on each side was 7 Å (r) [23]. For calculating the exchange-correlation functional generalized gradient approximation (GGA) was used as suggested by Perdew, Burke, and Ernzerhof [29]. Double zeta plus polarization basis sets were used to perform the necessary calculations.

In a two-probe configuration, the miller indices were taken as 1:1:1 [24]. The length of the unit cell along the c direction was taken to be 45 Å because this is the minimum length needed to insert a BNO between electrodes. To perform the necessary transport calculations and study the I-V curve Landauer-Buttiker formalism has been used [25].

$$I(V) = 2\frac{e}{h}\int_{\mu_L}^{\mu_R} T(E,V)[f(E-\mu_L) - f(E-\mu_R)]dE \qquad (1)$$

Where V represents the applied bias voltage, μ_L and μ_R denotes the electrochemical potential of left and right electrodes, and T (E, V) signifies transmission function respectively. T (E, V) is the transmission function that can be demonstrated from the information of coupling amongst the electrodes and the position of molecular energy levels. The transmission can be determined as follows [26].

$$T^k(E,V) = T_r[E,V)G_M^k(E,V)\Gamma_2^k(E,V)G_M^k(E,V) \quad (2)$$

The above equation $\Gamma(E)$ demonstrates the coupling function. It provides information regarding the form of contact between the molecule and the electrodes. G_M (E, V) signifies green's function. It can be assumed that devices can be divided into two interfaces, having two different chemical potentials. Thus, molecular energy levels tend to float above electrostatic potential. Conversely, it tends to float downwards. The magnitude of electrostatic potentials on both sides of electrodes can be determined as [27]

$$\mu_L = E_F - eV_{mol} = E_F - \eta eV \quad (3)$$

$$\mu_R = E_F - eV + eV_{mol} = E_F + (1-\eta)eV \quad (4)$$

Where e represents the charge on the electron, E_F denotes equilibrium Fermi energy and η describes the potential profile of the molecules in two probe configurations.

Next, the transmission pathways were calculated, which describes the flow of current through the molecular junction [28]. To get an insight into electron transfer rate the local currents that are bridging between the molecule and metallic leads were investigated. Local currents for a device have been examined through electrode-molecule-electrode systems. The sum of local currents is given as:

$$I(V) = \sum_{mn} I_{mn}(V) \quad (5)$$

Where m is atoms on one side of the electrode and n is on the other side. The transmission components are represented in form of arrows. Red arrows demonstrate the positive value of current when the transmission is from the first atom to the second atom. Blue arrows demonstrate components in opposite values, thereby reducing the net current.

3. Results and Discussion

First of all, the I-V curve was analyzed for both silicene and boron-based devices at various voltages ranging from -1V to +1V with a step size of 0.2V. From fig. 1, a comparison can be drawn that with an increase in bias, current decreases for silicene device on the contrary it increases for B_{40} devices. From figure 1, it is clear that all three molecular junctions have linear behavior, which signifies that the current flows without any barrier across the junction. From the I-V curve, it is deduced that the lowest value of current is observed in the $B_{20}@B_{40}$ device and the highest value for $N_{20}@B_{40}$. Also, a higher number of transmission peaks can be seen for $N_{20}@B_{40}$ which corresponds to the greater probability of transmission. The current values for the $C_{20}@B_{40}$ device range from -147872.88 to 147965.11nA, for $N_{20}@B_{40}$ range from -180475.436 to 187804.21nA, for $B_{20}@B_{40}$ range from -118060.61 to 115258.59nA respectively. The current values for all the devices increase as the value of bias increases. From the graph, we can anticipate the highest value of current in the $N_{20}@B_{40}$ device, which corresponds to reduced HLG when compared to other devices as shown in the table I. After analyzing the I-V curve for both the devices it is deduced that boron-based devices are better than silicene. Therefore, to get deeper insights into why boron-based devices are better transport properties of boron-based devices were calculated.

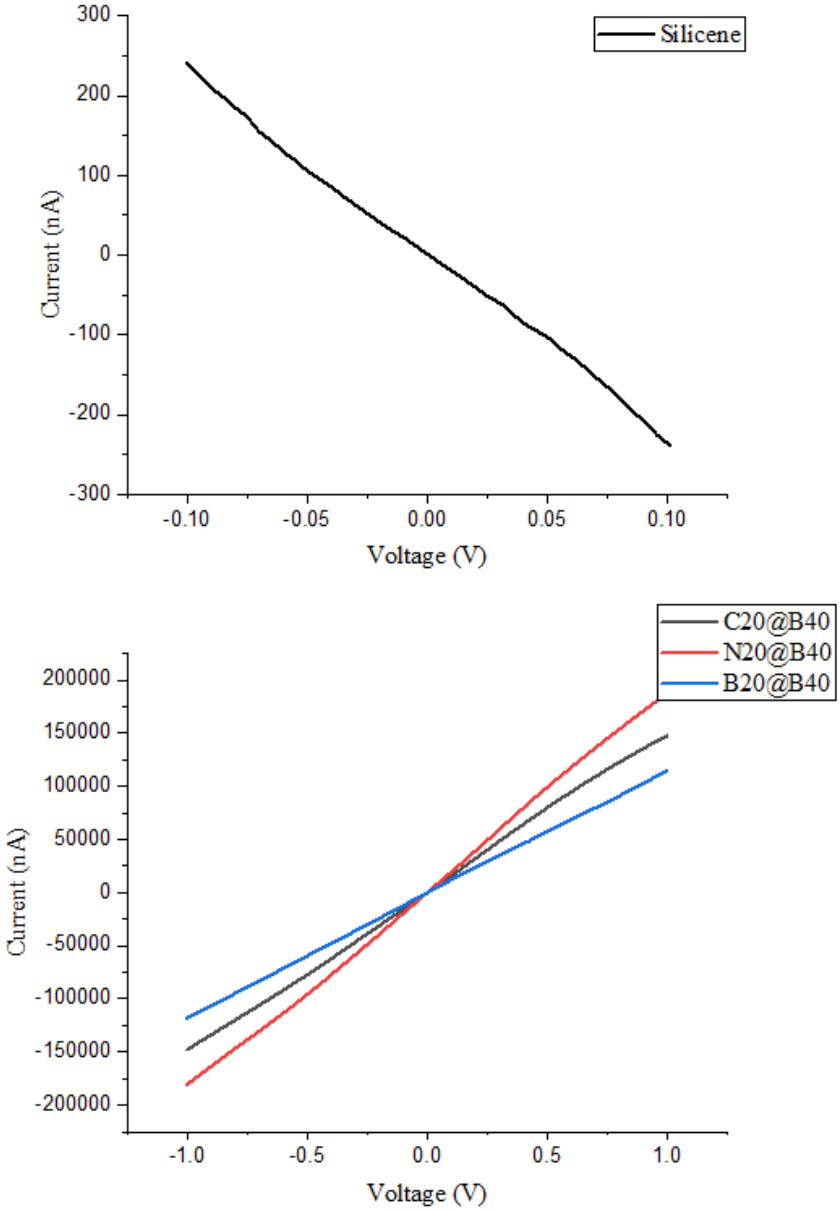

Fig.1: (a) I-V curve for Silicene device [30] (b) I-V curve for all BNO devices.

To understand quantum transport, it is necessary to analyze molecular junctions at various biases both in opposing directions. Thus, transmission spectra were not only analyzed at zero bias, but at various biases ranging from -1V to +1V with a step size of 0.2 V. From figure 2, we anticipate that peaks don't change their position for all three devices, but amplitude is varied. In the case of $N_{20}@B_{40}$ peaks don't change their position as we move from negative bias to positive bias but interestingly amplitude of the peak is increased in positive bias at various bias voltages. Whereas in the case of $C_{20}@B_{40}$ and $B_{20}@B_{40}$ amplitude of the peak is highest for negative bias and it gets reduced as we move towards positive bias. This transport behavior can be seen in the I-V curve also.

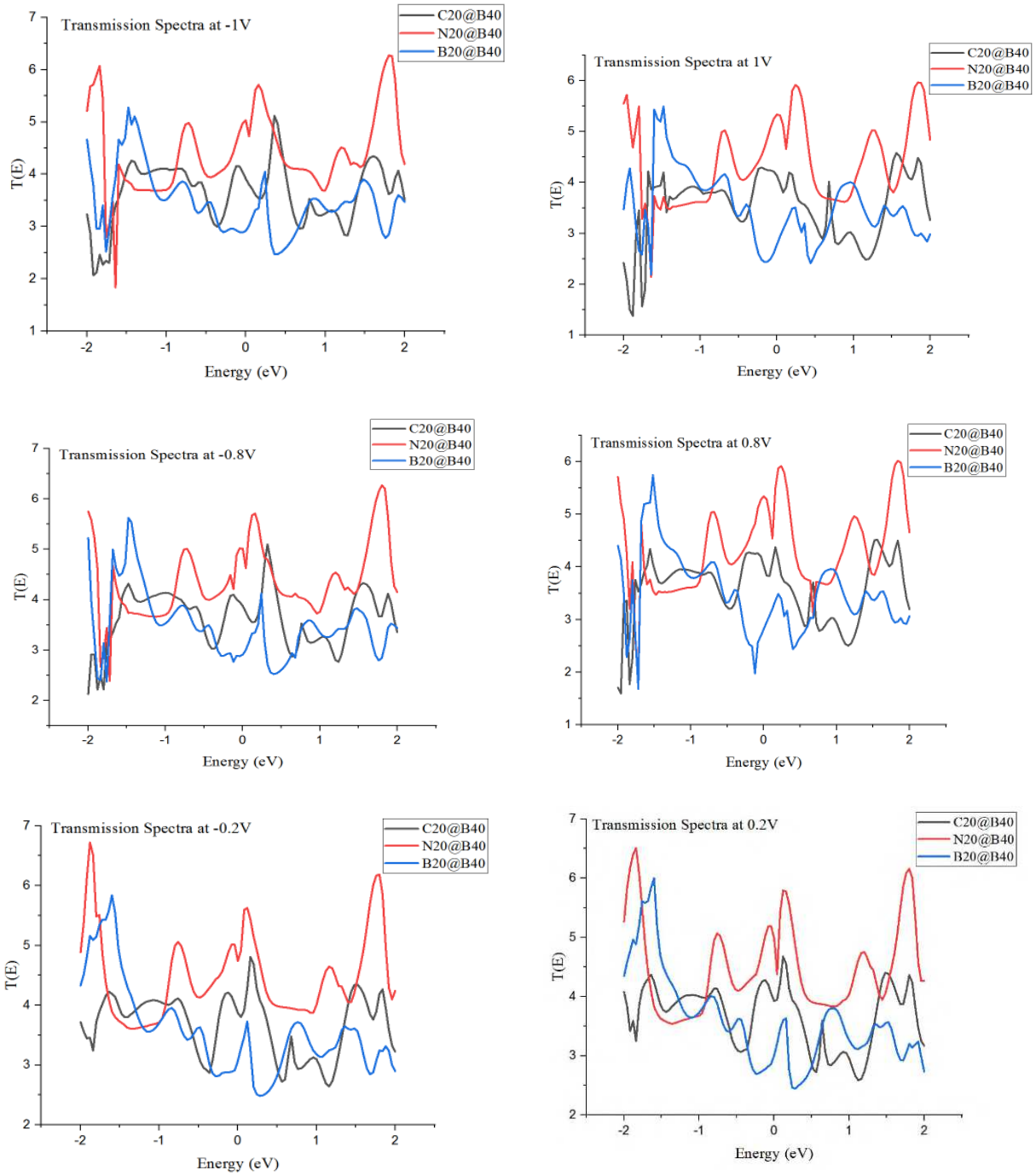

Fig.2: Transmission Spectra at various bias voltages.

Further, to understand transport properties at equilibrium, we firstly probe the density of states for all molecular junctions. The density of states gives information regarding the number of electron states that are vigorously taking part in transmission. Figure 3 shows the comparison between the density of states for three devices that are computed from PBE-DFT parameterization. Higher peaks are observed only on one side of the Fermi level. From the figure, it is visible that LUMO dominates the transmission for all three devices as peaks above E_F are more prominent. Border

peaks signify better transmission, which also gives us the information that bonding between the central molecule and metallic leads is reliable.

Furthermore, to understand the type of synergy between the molecule and electrodes at which energy transfer of electrons is prominent transmission spectra curve is analyzed at equilibrium. It is the transmission spectra that provide the information about the HLG gap and molecular orbitals that participate actively in transmission. Figure 4 shows the transmission spectra curves at zero bias for $C_{20}@B_{40}$, $N_{20}@B_{40}$, and $B_{20}@B_{40}$. In the case of all three devices, LUMO orbital dominates the quantum transport at E_F=0. Broader peaks above the E_F can be seen in the case of $B_{40}N_{20}$, thus implying stronger coupling resulting in greater transmission. Thus, the results derived from DOS and transmission spectra are in consensus.

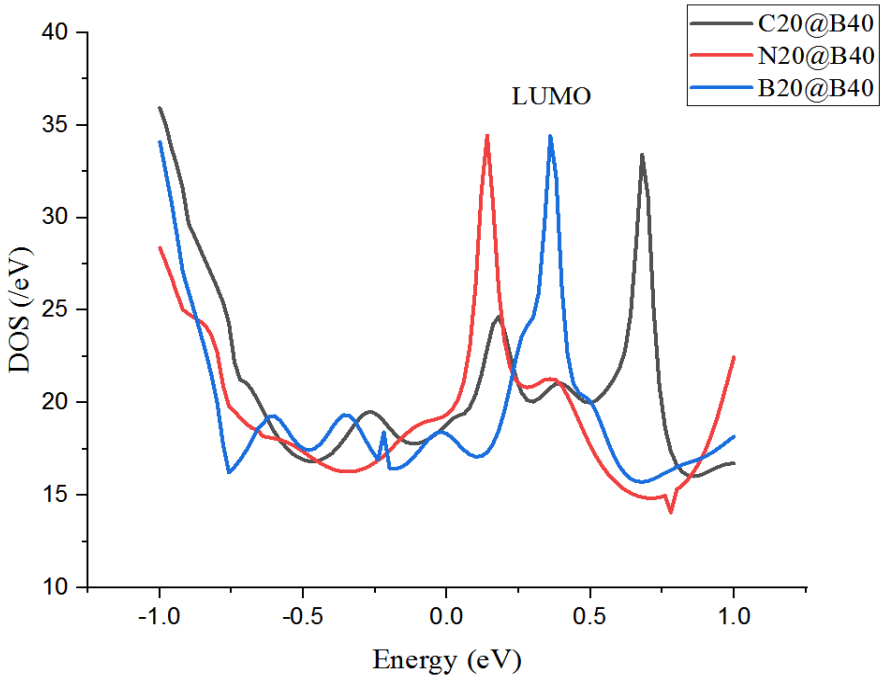

Fig.3: Comparison of density of states for $C_{20}@B_{40}$, $N_{20}@B_{40}$, and $B_{20}@B_{40}$.

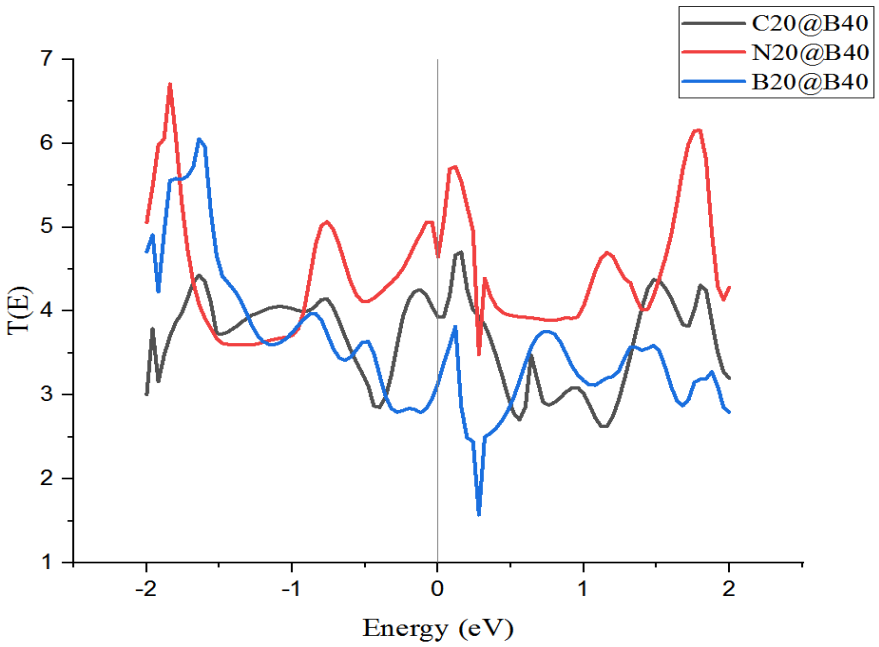

Fig.4: Transmission Spectra at 0V for all three devices under consideration.

Next, the molecular energy spectrum for $C_{20}@B_{40}$, $N_{20}@B_{40}$, and $B_{20}@B_{40}$ at 0V is considered. Table I gives information about HOMO, LUMO, and HLG for all the devices. From the table, it is deduced that on the placement of N_{20} in the fullerene cage HLG is reduced in comparison with the other two devices. The reduced HLG corresponds to the higher transmission. For the $N_{20}@B_{40}$ device, the HLG reduces as the active orbitals have more domination on charge transfer and are close to the Fermi level. These results also correspond to DOS as LUMO of $N_{20}@B_{40}$ is close to Fermi level followed by $B_{20}@B_{40}$ and then $C_{20}@B_{40}$. The HLG gap for the devices is calculated to be $C_{20}@B_{40}$ (0.226 eV) > $B_{20}@B_{40}$ (0.182 eV) > $N_{20}@B_{40}$ (0.097 eV). These results of the molecular energy spectrum are in correlation with the deductions from DOS analysis.

TABLE I HOMO, LUMO, and HLG for the three nano-onions

Device	HOMO	LUMO	HLG
B40-C20	-0.06855439	0.1576649	0.226
B40-N20	-0.04672549	0.05043612	0.097
B40-B20	-0.07601179	0.106059	0.182

To investigate the lower Homo-Lumo gap in $N_{20}@B_{40}$, the electron density for all three molecular junctions was contemplated. From figure 5 it can be seen that the electron cloud is more oriented around the N atoms of nitrogen variant onion in comparison with the other two onions. The high electron density is found on N atoms because of its large electro-negativity. The influence of the highest electron density in nitrogen variant onion can be seen on HLG, which implies that higher electron density on nitrogen atoms leads to reduced HLG. The results of electron density coincide with the results of the I-V curve, as nitrogen has the highest electron density as well as the highest value of current.

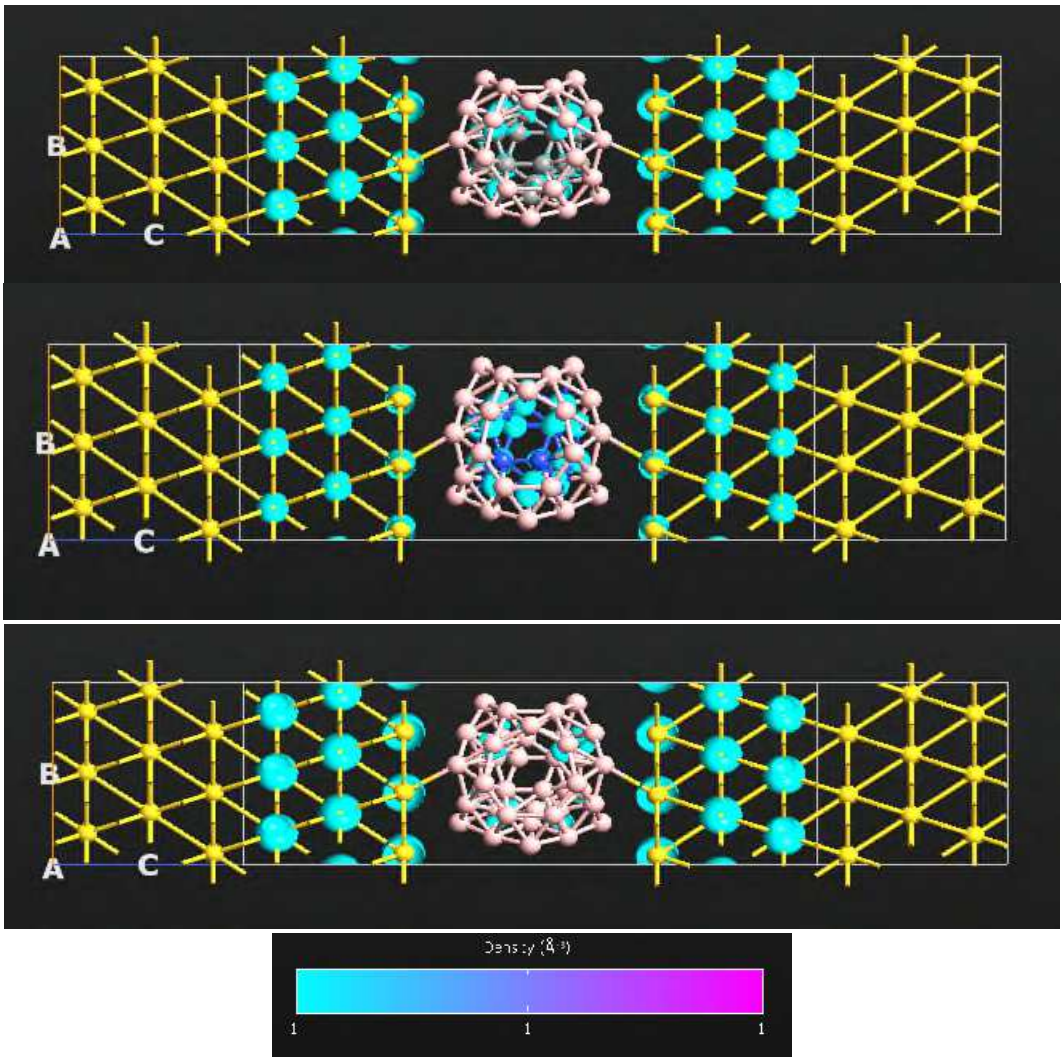

Fig.5: Electron density (a) $C_{20}@B_{40}$, (b) $N_{20}@B_{40}$, and (c) $B_{20}@B_{40}$.

Furthermore, the differential conductance of all three devices was calculated. From figure 6, it is evident that all three devices have different differential conductance. Higher value peaks are in positive bias and lower value peaks are seen in negative bias which is similar to the I-V curve in terms of the amplitude. B_{40} based nano-onion with nitrogen variant is perceived to have the highest differential conductance value followed by carbon variant and boron variant have the least conductance. It is contemplated that the $N_{20}@B_{40}$ device exhibits peak conductance at 0.29V which is about 20.4μS similar to the $C_{20}@B_{40}$ device conductance peak at 02.V which is about 16.2 μS. Hence results attained from differential conductance correspond with the results for the I-V curve and transmission pathways.

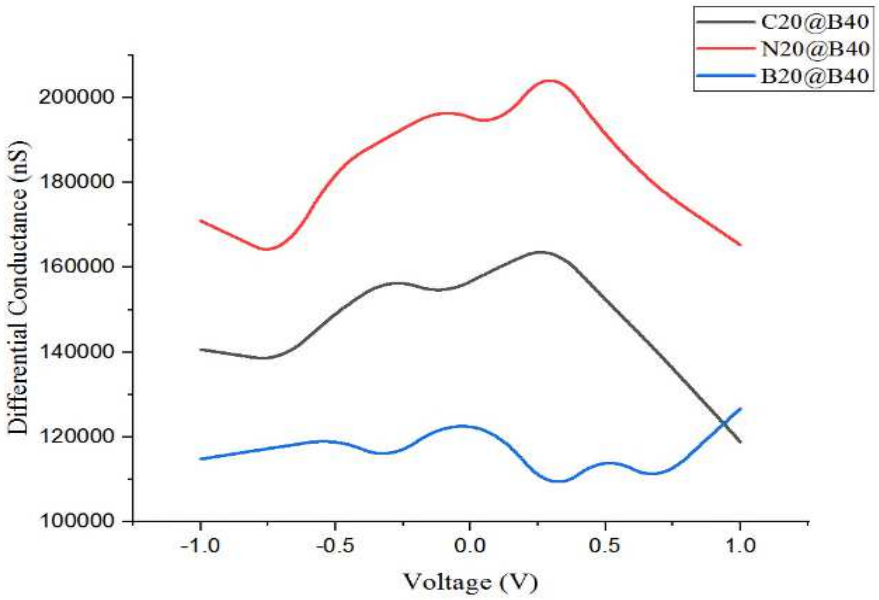

Fig.6: Comparison of differential conductance (a) $C_{20}@B_{40}$, (b) $N_{20}@B_{40}$, and (c) $B_{20}@B_{40}$.

The Transmission Pathways is a quantitative option that separates the transmission coefficient into local bond contributions, T_{ij}. The pathways have the ability that if the system is divided into two parts, then pathways across the boundary between A and B sum up to the total transmission coefficient.

$$T(E) = \sum_{i\epsilon A, j\epsilon B} T_{ij}(E)$$

The local bond contributions, T_{ij} can be both positive and negative. A negative value represents that the electron is backscattered along the bond. In many systems, there will be a single pathway that dominates the flow of transmission whereas in many systems there will be multiple pathways that contribute to the flow of transmission. The direction of arrows shows the flow of electrons. The red arrow corresponds to the positive value of current, whereas the blue arrow corresponds to a reduction in current. On the other hand, the purple arrow represents the backscatter of electrons. From figure 7, it can be seen that the case of the $N_{20}@B_{40}$ onion has a greater number of red arrows which implies that transmission is positive thus leading to more value of current. In the case of $C_{20}@B_{40}$ and $B_{20}@B_{40}$ large number of blue and purple arrows signify a lesser value of current. Backscattering can be seen in all three devices but $N_{20}@B_{40}$ has the least amount of backscattering. From the fig.7, it is visualized that flow of current is mainly inside the fullerene cage. The fullerene cages of N_{20}, C_{20}, and B_{20} act as a bridge during electron transmission which contributes to more number of channels thus increasing the conductance. Our results of transmission pathways are in agreement with the current-voltage results which demonstrate that $N_{20}B_{40}$ has the highest value of current.

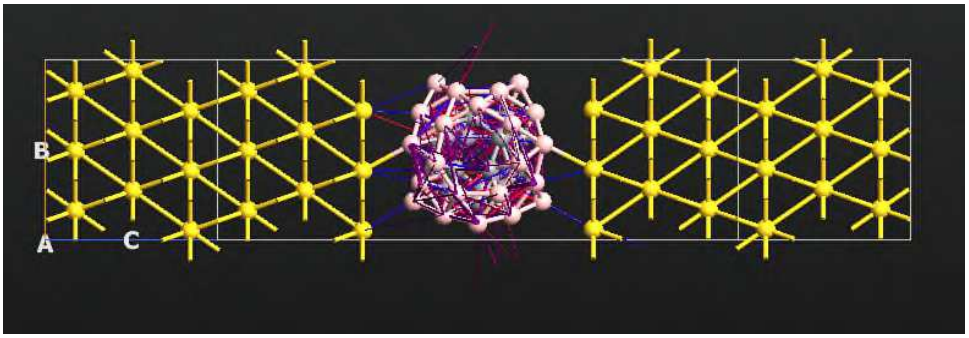

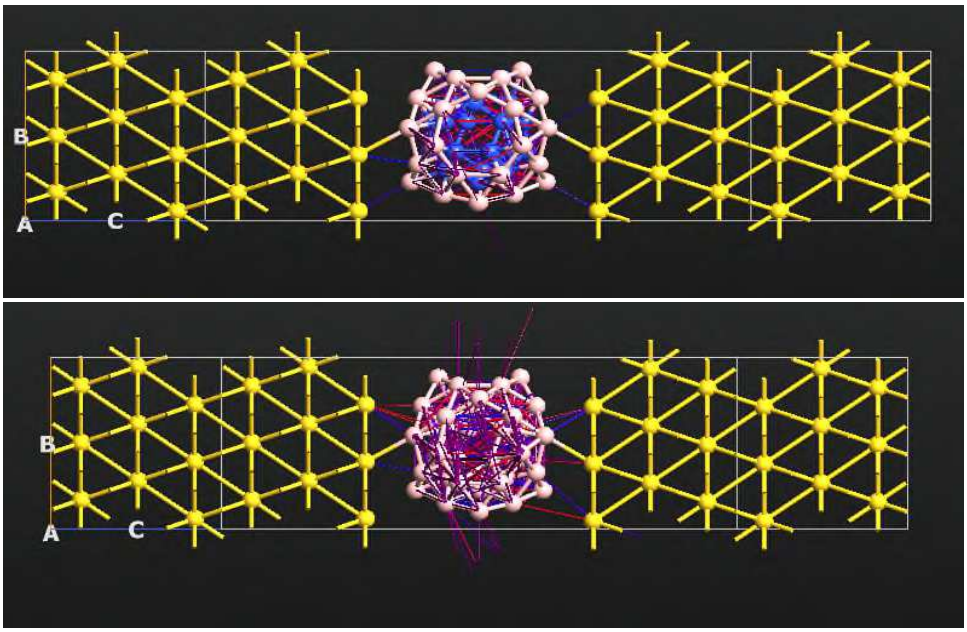

Fig.7: Transmission pathways for (a) $C_{20}@B_{40}$, (b) $N_{20}@B_{40}$, and (c) $B_{20}@B_{40}$.

Conclusion

In this research work, we envisage the Silicene and Boron nano-onion formulated by infusing the C_{20}, N_{20}, and B_{20} into B_{40} fullerene. DFT with NEGF duo has been utilized to calculate DOS, HLG, molecular spectrum, electron density, I-V curve, and differential conductance of $C_{20}@B_{40}$, $N_{20}@B_{40}$, and $B_{20}@B_{40}$. It was found that with an increase in bias current decreases for silicene devices on the contrary it increases for B_{40} devices. From investigating DOS, it is inferred that for all the devices under study LUMO orbitals play dominance in transmission. The $N_{20}@B_{40}$ nano-onion has the highest value of current ranging from -180475.436 to 187804.21nA in comparison to the other two devices. This is due to the reduced HLG as well as higher electron densities. The HLG gap for the devices is calculated to be $C_{20}@B_{40}$ (0.226 eV) > $B_{20}@B_{40}$ (0.182 eV) > $N_{20}@B_{40}$ (0.097 eV). Thus, infusing N_{20} in B_{40} fullerene leads to improvement of current in BNO junction.

Acknowledgment

The authors acknowledge the university with the potential for Excellence (UPE) scheme of UGC for providing us the computational facility of Virtual Nano Lab in Guru Nanak Dev University, Amritsar for carrying out this research work.

This research work did not receive any specific grant from funding agencies in the public, commercial, or not-for-profit sectors.

Declarations

Funding: This research does not receive any specific grant from funding agencies in the public, commercial, or not-for-profit sectors.

Conflict of interest/Competing interests: on behalf of all the authors, the corresponding author states that there is no conflict of interest.

Ethics approval: N/A

Consent for publication: All authors give their consent.

Consent to participate: All authors give their consent.

Availability of data and material: N/A

Code availability: N/A

Authors' contributions: Harleen Kaur came up with the idea, wrote the introduction section and performed the necessary modeling and simulations, and analyzed the results. Jupinder Kaur interpreted the results and proof-read the manuscript. Ravinder Kumar interpreted the results and edited the manuscript.

REFERENCES

1. The Nobel Prize in Physics (1956) http://www.nobelprize.org/nobel_prizes /physics/laureates/1956/accessed 4 Jul 2013.
2. J.A. Hoerni (1960), "Planar Silicon Transistors and Diodes, IRE Electron Dev. Mtg., Wash., D.C., Oct, 1960
3. 3 J.A. Hoerni (1961), Planar Silicon Devices and Transistors, Transactions on Electron Devices, ED-8, 178
4. 4 J. A. Hoerni (1962), "Method of Manufacturing Semiconductor Devices, U.S. Patent No. 3,025,589", Filed May 1, 1959, Issued March 20
5. **R.P. Feynman**, 'There is plenty of room at the bottom', Eng. Sci., vol. 23, pp. 22-36, 1960.
6. Gian G. Guzmán-Verri and L. C. Lew Yan Voon, "**Electronic structure of silicon-based nanostructures", Phys. Rev. B** 76**, 075131 – Published 30 August 2007,** DOI:https://doi.org/10.1103/PhysRevB.76.075131
7. Z. G. Shao, X. S. Ye, L. Yang,and C. L. Wang, J. Appl. Phys. **114**, 093712 (2013).
8. Electrical properties of silicon, Ioe Institute Database.
9. Wella, Sasfan & Syaputra, Marhamni & Wungu, Triati & Suprijadi, Suprijadi. (2016). The study of electronic structure and properties of silicene for gas sensor application. AIP Conference Proceedings. 1719. 030039. 10.1063/1.4943734.
10. Zou, Dongqing & Zhao, Wenkai & Fang, Changfeng & Cui, Bin & Liu, D.s. (2016). The electronic transport properties of zigzag silicene nanoribbon slices with edge hydrogenation and oxidation. Phys. Chem. Chem. Phys.. 18. 10.1039/C6CP01159D.
11. DavoodianIdalik, M. & Kordbacheh, A. & Ghasemi, Narges. (2018). Electronic, magnetic and transport properties of silicene armchair nanoribbons substituted with monomer and dimer of Fe atom. AIP Advances. 8. 065207. 10.1063/1.5029426.
12. Jiang, Q. G. and Zhang, J. F. and Ao, Z. M. and Wu, Y. P, "Density functional theory study on the electronic properties and stability of silicene/silicane nanoribbons"J. Mater. Chem. C, http://dx.doi.org/10.1039/C4TC02829E
13. Zhai, H.J., Zhao, Y.F., Li, W.L., Chen, Q., Bai, H., Hu, H.S., Piazza, Z.A., Tian, W.J., Lu, H.G., Wu, Y.B., Mu, Y.W., Wei, G.F., Liu, Z.P., Li, J., Li, S.D. and Wang, L.S., 2014. Observation of an all-boron fullerene. *Nature Chemistry, 6*, pp.727–731.
14. Fa, W., Chen, S., Pande, S. and Zeng, X.C., 2015. Stability of metal encapsulating boron fullerene B40. *The Journal of Physical Chemistry A, 119*(45), pp.11208–11214.
15. Yang, Z., Ji, Y.L., Lan, G., Xu, L.C., Liu, X. and Xu, B., 2015. Design molecular rectifier and photodetector with all boron fullerene. *Solid State Communications, 217*, pp.38–42.
16. An, Y., Zhang, M., Wu, D., Fu, Z., Wang, T. and Xia, C., 2016. Electronic transport properties of the first all-boron fullerene B40 and its metallofullerene Sr@B40. *Physical Chemistry Chemical Physics, 18*, pp.12024–12028.
17. Vohra, R., Sawhney, R.S., Kaur, J. *et al.* Adenine based molecular junction as biosensor for detection of toxic phosgene gas. *J Mol Model* **26,** 172 (2020). https://doi.org/10.1007/s00894-020-04427-z
18. Lang ND (1995) Resistance of atomic wires. Phys Rev B Condens Matter Mater Phys 52(5335)

19. Xue Y, Datta S, Ratner MA (2002) First-principles based matrix Green's function approach to molecular electronic devices: general formalism. Chem Phys 281(151)
20. Brandbyge M, Mozos JL, Ordejon P, Taylor J, Stokbro K (2002) Density-functional method for non-equilibrium electron transport. Phys Rev B Condens Matter Mater Phys 65(165401)
21. Taylor J, Guo H, Wang J (2001) Ab initio modeling of quantum transport properties of molecular electronic devices. Phys Rev B Condens Matter Mater Phys 63(245407)
22. Atomistic Toolkit Manual, Quantumwise Inc. Atomistix toolkit version 13.8.0, Quantumwise A/S (http://quantumwise.com)
23. Y.P. An, M. Zhang, D. Wu, Z. Fu, T. Wang, C. Xia, Phys. Chem. Chem. Phys., vol. 18, pp. 12024-12028, 2016.
24. V. Rodrigues, T. Fuhrer, and D. Ugarte: Signature of atomic structure in the quantum conductance of gold nanowires. Phys. Rev. Lett. 85, 4124 (2000).
25. R. Landauer: Conductance determined by transmission: Probes and quantized constriction resistance. J. Phys.: Condens. Matter 1, 8099 (1989).
26. J. Heurich, J.C. Cuevas, W. Wenzel, and G. Schon: Electrical transport through single-molecule junctions: From molecular orbitals to conduction channels. Phys. Rev. Lett. 88, 256803 (2002).
27. J.W. Lawson and C.W. Bauschlieher: Transport in molecular junctions with different metallic contacts. Phys. Rev. B: Condens. Matter Mater. Phys. 74, 125401 (2006).
28. Solomon, G., Herrmann, C., Hansen, T. *et al.* Exploring local currents in molecular junctions. *Nature Chem* **2,** 223–228 (2010). https://doi.org/10.1038/nchem.546
29. J.P. Perdew, K. Burke, and M. Ernzerhof: Generalized gradient approximation made simple. Phys. Rev. Lett. 77, 3865 (1996).
30. Zhou, Ruiping "Structural And Electronic Properties of Two-Dimensional Silicene, Graphene, and Related Structures", http://rave.ohiolink.edu/etdc/view?acc_num=wright1341867892